actuators

MDPI

Article

Maskless Writing of Surface-Attached Micro-Magnets by Two-Photon Crosslinking

Nicolas Geid [1,2], Jan Ulrich Leutner [1], Oswald Prucker [1] and Jürgen Rühe [1,2,*]

[1] Department of Microsystems Engineering (IMTEK), University of Freiburg, Georges-Köhler-Allee 103, D-79110 Freiburg, Germany
[2] Cluster of Excellence livMatS @ FIT–Freiburg Center for Interactive Materials and Bioinspired Technologies, Georges-Köhler-Allee 105, D-79110 Freiburg, Germany
* Correspondence: ruehe@imtek.de

Abstract: Surface-bound 3D micro-magnets are fabricated from photoreactive copolymers filled with magnetic nanoparticles by maskless 3D writing. The structures are generated by 2-photon crosslinking (2PC), which allows direct writing into solid films of composites consisting of magnetic particles and a photoreactive elastomer precursor. With this strategy, it is possible to directly write complex, surface-bound magnetic actuator structures, which generates new opportunities in the fields of microfluidics and bioanalytical systems. Compared to the common 2-photon polymerization, in which the writing process takes place in a liquid resin, the direct writing based on the 2PC method takes place in a solid polymer film (i.e., in the glassy state).

Keywords: micro-actuators; two-photon lithography; two-photon crosslinking; photoreactive polymers; micro-magnets

Citation: Geid, N.; Leutner, J.U.; Prucker, O.; Rühe, J. Maskless Writing of Surface-Attached Micro-Magnets by Two-Photon Crosslinking. *Actuators* **2023**, *12*, 124. https://doi.org/10.3390/act12030124

Academic Editor: Richard Yongqing Fu

Received: 7 February 2023
Revised: 6 March 2023
Accepted: 10 March 2023
Published: 15 March 2023

1. Introduction

Micro-actuators are very interesting systems both from an academic as well as from an application-oriented point of view as they allow the generation of large fields of actuators which can work in concert. They can be used to generate coordinated and cooperative movements and, thus, allow the development of novel devices and systems [1,2]. Such systems are particularly attractive for microfluidic pumping and mixing and even more so for complex active stimulation of biological systems, including those that involve cell stimulation [3]. A strong inspiration for the design of micro-actuators has frequently been ciliated organisms in nature, which use the movement of tiny hairs to move liquid. Many different methods have been developed to mimic such ciliated organisms using micro-actuators and actuator fields, frequently called artificial cilia [4–7]. These synthetically generated actuators react to different external stimuli, e.g., to electrostatic [8], light [9,10], piezo [11] and magnetic actuation [6,12–15]. Magnetic actuation is particularly suitable because the process can be well controlled and the weak interaction of magnetic fields with biological materials usually causing only minor perturbations [16,17]. Magnetic micro-actuators generally consist of magnetic particles which are incorporated in elastomers. In most cases, mask- or mold-based processes are employed to form the magnetic microstructures [14,18,19]. Published work on artificial cilia shows that high pumping efficiencies and controlled particle transport can be achieved by actuation with an external magnetic field [20,21]. In addition to mold-based processes, a mask-based two-color lithography process based on C,H insertion crosslinking has recently been described for the generation of magnetic microflaps, which have been incorporated into microfluidic chips. These actuators achieved average flow velocities of hundreds of µm/s, which shows that effective pumping rates can also be achieved with such a materials system [14,22,23].

Micro-molding [24] and mask-based techniques are standard technologies and allow the generation of large actuator fields. However, they are limited when it comes to the

generation of more complex geometries that vary locally, which is required in more demanding applications, such as when cooperative action is needed. Molding processes, for example, cannot produce undercut or other complex structures, such as spherical objects, where demolding is difficult or even impossible. Further, in such processes, it is difficult to implement local variations in the chemical composition or mechanical properties of the actuators, e.g., produce structures with variations in stiffness. Additionally, for all design changes of the structure, a new mold needs to be generated which makes complex studies with frequent structural redesign tedious. In contrast to this, a direct writing process allows the flexible selection of 3D designs for actuators, giving full control in the manufacturing of complex and eventually cooperative actuator systems.

A direct writing process that has received much attention in recent years is 2-photon lithography [25–27], in which high-resolution microstructures are usually written by 2-photon polymerization using a femtosecond laser [28–32]. In such processes, the 2-photon activation is used to locally initiate a polymerization reaction leading to the formation of polymers or a polymer network in the illuminated volume element (voxel) [33]. A variety of freely swimming micro-actuators generated using 2-photon polymerization has been described. Such systems are of great interest, especially in the field of medical microrobots [34–36]. Recent publications have also considered the writing of surface-attached magnetic micro-springs using 2-photon polymerization, which could be moved with the help of a magnetic field. In this process, 2.1 wt.% Fe_3O_4 nanoparticles were introduced in a monomer resin [37,38].

Recently, a new technique in 2-photon lithography called 2-photon crosslinking has been introduced, which represents an attractive alternative to the commonly used 2-photon polymerization process [39]. In this method, copolymers are used which are equipped with a photochemically reactive group and can be simultaneously crosslinked and surface-bonded by 2-photon excitation in the glassy state using C,H insertion chemistry [39]. Compared to 2-photon polymerization, several layers of different polymers can be applied on top of each other, resulting in a multifunctional material [40]. This technique uses no monomeric compounds, which is very attractive from a safety point of view for working in an optics laboratory. Additionally, as the polymer can be thoroughly purified before use, the final structures are monomer-free, which is very important for any biological or biomedical application. Quality control with respect to the contents of residual monomers in additive manufacturing processes based on polymerization reactions is difficult to ensure as only single objects are generated. This is potentially a serious problem as the monomer content depends very strongly on the details of the conditions under which the writing process is performed [39,41].

Following up on this concept, we present here a novel method for the direct writing of micro-magnets using 2-photon crosslinking (2PC), based on a photoactive elastomeric copolymer with magnetically embedded nanoparticles. A schematic illustration of this process is shown in Figure 1b,c. As described, the process is based on 2-photon absorption in a small volume around the focal point (voxel), which eventually leads to formation of a polymer network via a C,H insertion crosslinking (CHic) reaction. The very same reaction leads to a surface-attached layer if the surface of the substrate is first decorated with an alkyl silane layer [40–43]. The non-crosslinked polymer is easily removed using a suitable solvent, and the written microstructures remain on the surface as they are covalently linked to the substrate. We will also show how the resulting layers can be actuated using a rotating magnet which is operated below the substrate and discuss the resulting deflections of the micro-actuators based on simple Euler–Bernoulli beam theory [44,45].

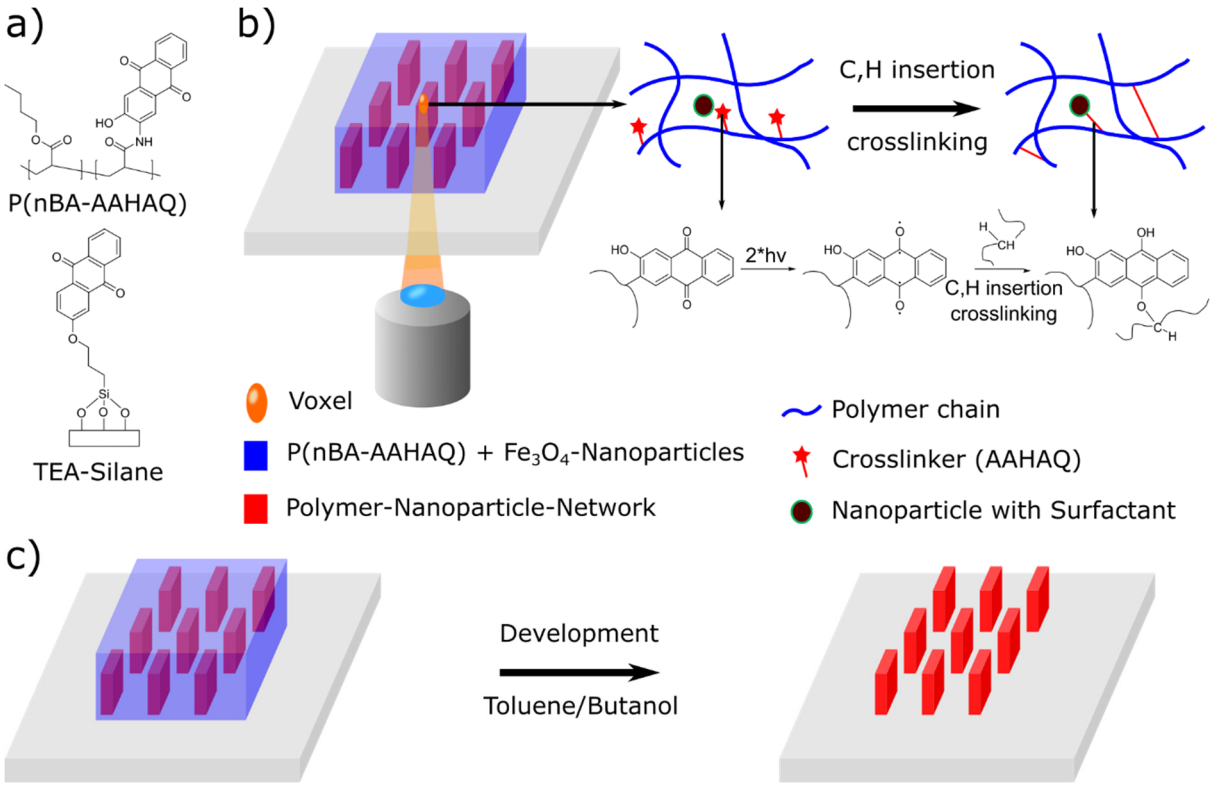

Figure 1. (**a**) Molecular structures of the copolymer P(nBA-AAHAQ), and the triethoxy anthraquinone silane (TEA-silane) used for a covalent attachment to the glass slide. (**b**) Schematic representation of the 2-photon crosslinking process. The femtosecond laser triggers a C,H insertion crosslinking reaction within a small volume (voxel) in the solid, nanoparticle containing, polymer layer. The formation of a polymer network and the incorporation of the nanoparticles result in the writing of three-dimensional structures from bottom to top. (**c**) By developing in a suitable solvent (e.g., toluene/butanol), the non-crosslinked polymer chains are washed out and the micro-actuators are obtained.

2. Materials and Methods

Materials: 2-Amino-3-hydroxyanthraquinone was purchased from TCI, Germany. All other chemicals were purchased from Sigma Aldrich, Germany. Dimethyl acrylamide and n-butylacrylate (nBA) were purified by filtration through basic aluminum oxide and distillation. 2,2′-Azobis(2-methylpropionitrile) (V70; Fujifilm Wako Chemicals Europe, Neuss, Germany) was recrystallized from ethanol. All other chemicals and solvents were used as received.

Photoreactive monomer: 2-Amino-3-hydroxyanthraquinone (2.39 g, 10.0 mmol, 1.0 eq) was dissolved in an inert gas atmosphere in 1,4-dioxane (100 mL). A solution of acrylic acid chloride (0.68 mL, 0.72 g, 8.0 mmol, 0.8 eq) in dioxane (20 mL) was added while stirring at 0 °C. After complete addition, the reaction mixture was heated for 6 h to reflux. Afterwards the reaction solution was filtered and the filter cake was taken up in ethanol (3 × 150 mL) and heated to reflux. The solid product was filtered off and dried under vacuum, resulting in a yellow product with a yield of 84% (1.97 g, 6.7 mmol).

^{1}H-NMR (250 MHz, DMSO-d6, δ): 5.80 (dd, J = 2 Hz, 10 Hz, 1H), 6.35 (dd, J = 2 Hz, 17 Hz, 1H), 6.87 (dd, J = 10 Hz, 17 Hz, 1H), 7.63 (s, 1H, Ar-H), 7.82–7.94 (m, 2H, Ar-H), 8.10–8.22 (m, 2H, Ar-H), 9.05 (s, 1H, Ar-H), 9.81 (s, 1H, OH), 11.71 (s, 1H, NH).

^{13}C-NMR (250 MHz, DMSO-d6, δ): 112.51 (C3), 119.90 (C6), 126.71 (C5), 127.34 (C11), 127.49 (C14), 128.84 (C17), 130.77 (C13), 132.51 (C12), 133.09 (C1), 133.96 (C16), 134.15 (C8), 134.88 (C9), 135.17 (C2), 153.38 (C4), 164.92 (C15), 182.36 (C7), 182.75 C10).

Photocurable copolymer: The copolymer was synthesized via free radical polymerization with 92.5 mol% nBA and 7.5 mol% 2-amino-3-hydroxyanthraquinone (AAHAQ)

at 30 °C with the V70 initiator. Reaction time: 24 h, yield 70%. The AAHAQ content was determined to be 7.4% according to NMR spectroscopy based on the integration of the signals due to the aromatic protons (7.6–7.9 ppm). According to the GPC data, the molecular masses of the obtained copolymers were M_n = 93.000 g/mol and M_W = 241.000 g/mol, so that the polymers carried, on average, approximately 70 AAHAQ repeat units per polymer chain.

Magnetic resin: The photo-cross-linkable magnetic composite was obtained by mixing 25 µL of commercial Fe_3O_4 superparamagnetic ferrofluid (EMG 905 containing oleic acid as stabilizer, Ferrotec, NH, Bedford, MA, USA) in a solution of 100 mg photocurable copolymer P(nBA-7.5%AAHAQ) in 0.975 mL toluene to obtain a homogenous dispersion.

Fabrication process of the micro-actuators: For the fabrication of the magnetic micro-actuators, glass slides (22 × 22 mm, 170 µm thick) were first silanized with a 50 mM triethoxy anthraquinone silane ((TEA)-silane) in toluene. The synthesis of the TEA-silane was carried out according to [39]. The solution (100 µL) was applied to a glass slide and spin-coated at 1000 rpm for 30 s. For the surface attachment, it was heated to 120 °C for 30 min and the non-attached silane was washed out with toluene. To obtain a polymer nanoparticle layer of about 80–100 µm, 50–100 µL of the dispersion described above was drop-cast onto the treated glass slide. The toluene was slowly evaporated over 2 h at room temperature to avoid bubble formation. As soon as the layer had solidified, the remaining toluene could be removed by heating to 100 °C for 1 h. A 100 µm thick glassy polymer composite layer with approx. 10 wt.% nanoparticles was obtained. After completion of the 2-PC process, the substrates were placed in n-butanol and developed for at least 2 h, thus washing out the unreacted polymer.

Design of the micro-actuators: The beam-like micro-actuators were designed to have a height of 60–75 µm and a length of 20 µm. The thickness varied from 3 µm to 8 µm depending on the structure. The distance between two adjacent bars was 80 µm.

Direct writing of the magnetic micro-actuators: All structures were designed using Solidworks or Think3D computer programs to generate a stereolithography file (stl.). The 2-photon lithographs were performed using the Nanoone setup (UpNano GmbH, Vienna, Austria). It was equipped with a Ti-sapphire laser having a wavelength of 780 nm and a laser power of 500 mW. This printer uses a galvanometer scanning method. The generated stl. files were loaded into the Think3D version 1.7.3 software (Nanoone, UpNano GmbH, Vienna, Austria). For writing, a 20× magnification lens with 0.7 NA was used. Printing was performed in bottom-up mode and the lens was immersed into water. Slicing was set to 0.5 µm and hatching to 0.15 µm; a laser power of 15 mw and a scan speed of 100 mm/s were used.

Magnetic actuation and optical microscopy: A rotating permanent magnet was used to actuate the structures. This magnet had a field strength of 1.4 T (N42). The magnet was rotated by a motor at 30 rpm installed 1.5 cm below the stage of an optical microscope. With the help of a magnetometer, a maximum field strength of 130 mT was measured at the sample position. In this way, the structures could be made to move by the gradient of the magnetic field strength which ranged from 0 to 130 mT.

SEM: To prevent collapse, the structures kept in ethanol were dried using a critical point dryer (Leica EM CPD300, Wetzlar, Germany). The parameters chosen for the CPD were a cooling temperature of 10 °C, CO_2 in medium velocity, 16 exchange cycles, a critical temperature of 38 °C, and gas out medium velocity. Subsequently, scanning electron micrographs (5 kV, 0.1 nA) could be obtained using an FEI Scios 2 HiVac (Thermo Fisher, Waltham, MA, USA). The samples were gold-sputtered with a Cressington Sputter Coater 108auto. The images were taken at a 45° angle.

3. Results and Discussion

The material systems for the generation of the micro magnetic structures by 2-photon crosslinking processes consisted of superparamagnetic particles and a copolymer, which was composed of a matrix component and a photoreactive unit for crosslinking. As pho-

toreactive group 2-amino-3-hydroxyanthraquinone (AAHAQ) developed by Schwärzle et al. was chosen, which exhibits pronounced 2-photon absorption due to its designed electronic structure (i.e., conjugated π-system, planarity, donor and acceptor groups) [39]. Briefly, the photoreactive group AAHAQ was obtained in a one-step synthesis from 2-amino-3-hydroxyanthraquinone and acrylic acid chloride. The desired P(nBA-AAHAQ) copolymer (see Figure 1a) was prepared by free radical polymerization of N-buylacrylate (nBA) and AAHAQ at 30 °C using a low-temperature initiator (2,2′-azobis(4-methoxy-2,4-dimethylvaleronitrile (V70).

For the incorporation of the nanoparticles, particular attention must be paid to the compatibility of the particles and the copolymer. N-butylacrylate is a suitable soft component and an attractive component for biological applications, especially cell experiments [46]. Due to the hydrophobic nature of the nBA polymer, hydrophobically coated (i.e., oleic acid stabilized) iron nanoparticles were chosen, to allow sufficient miscibility. The copolymer and the nanoparticles were dispersed in toluene to form a homogeneous dispersion, which was stable between 0–20 wt.% content of nanoparticles. In order to obtain comparable results, in the following, we focus on dispersions with 10 wt.% nanoparticles.

For attaching the forming structures to the surfaces, a triethoxy anthraquinone silane (TEA-silane, see Figure 1a) was prepared and a self-assembled monolayer was formed on the glass surface. For the writing process, the dispersion was drop-cast onto the substrate to form a thin film of about 100 µm. Upon 2-photon illumination, the chromophore in the copolymer was excited into a triplet state and the polymer crosslinked through C,H insertion reactions (CHic). At the same time, the crosslinker units in those voxels in direct contact with the silane monolayer were also excited and attached to the forming network, so that the entire forming structure became covalently bound to the glass substrate. Moreover, the crosslinker molecules could probably also insert into the C,H bonds of the oleic acid molecules on the surface of the Fe_3O_4-nanoparticles, thus firmly binding the nanoparticles into the network. After writing the latent 3D image into the film, it was developed using n-butanol, a theta-solvent for the polymer. If a good solvent, such as toluene, was chosen instead, the structures formed became too strongly swollen, so that, in some cases, the swelling pressure became so great that they were torn off from the surface and the yield of perfectly formed structures was lower than that in the case where a solvent for the polymer was used as the developer, which was still capable of dissolving the polymer, but was of lower solvent quality. The micro-actuators were then transferred to ethanol in which the actuation took place. To dry the structures, i.e., for SEM imaging, in the case of high-aspect-ratio structures, critical point drying with CO_2 was employed. Since no meniscus formed during the drying process, a collapse of the structures was completely prevented, and large fields of perfectly shaped actuators were obtained.

To characterize the movement of micro-actuators written with the 2PC process, simple beam structures were investigated. A 20× water immersion objective with 0.7 NA was used for writing the micro-actuators. The writing parameters chosen for this material were a laser power of 15 mW, a writing speed of 100 mm/s, a hatching distance of 0.15 µm and a slicing distance of 0.5 µm. These parameters were used for all experiments described in this paper. Figure 2a shows a schematic representation of the deflection of the micro-actuators. A permanent magnet (N42) was rotated with a speed of 30 rpm under the micro-actuators, which responded to the gradient of the field lines. The magnetic flux density B in the y- and z-directions at the actuator position as a function of the rotation angle is shown in Figure 2b. The micro-actuators experienced a maximum magnetic flux density of 130 mT, which led to the desired deflection of the beams. Figure 2d shows the resulting deflection of the beams under investigation. The actuators not deflected are shown in the upper part of the figure, and the maximum deflected actuators are shown in the lower part of the figure. The beams shown here were printed with a width of 20 µm, a thickness of 3 µm and a height of 70 µm. In ethanol, the micro-actuators swelled by a factor of 1.2 but remained firmly attached to the substrate as they were covalently bound there. The actuator fields were practically free of defects, illustrating the high reproducibility of this manufacturing technique. Figure 2c

shows scanning electron microscope images that demonstrate the high resolution of the beam structures. As the specimens dried, they de-swelled, causing a slight decrease in volume. The drying process was also the reason for the slight rounding of the structures at the edges.

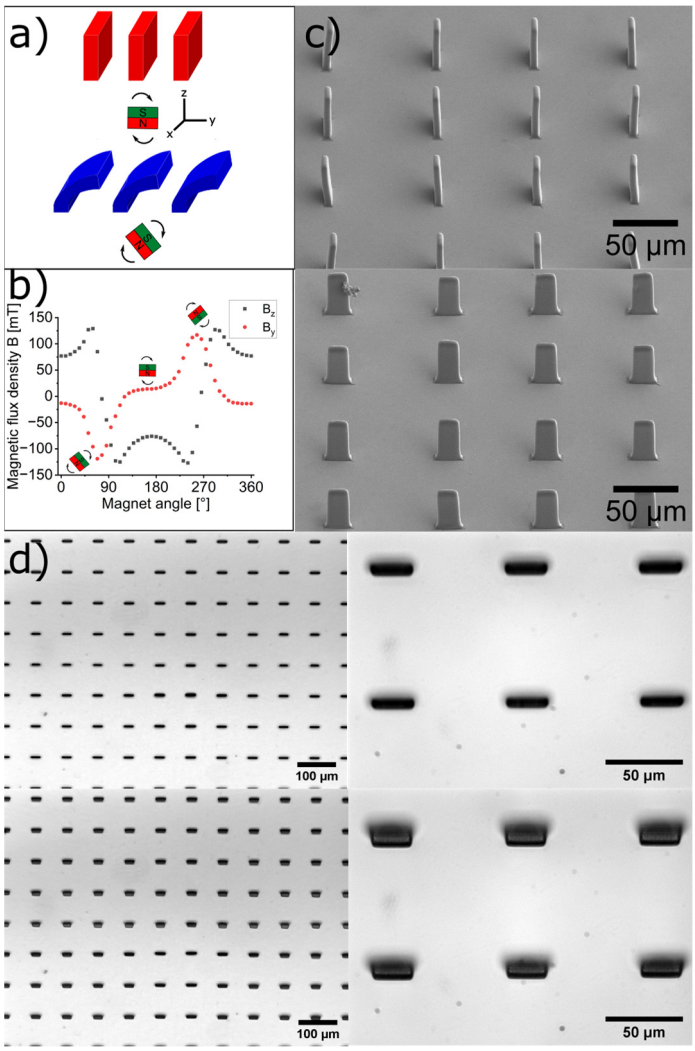

Figure 2. (**a**) Schematic representation of the deflection of beam structures by a rotating permanent magnet. (**b**) Graphical representation of the magnetic flux density B as a function of the rotation angle of the permanent magnet (N42). The permanent magnet was placed at a distance of 1.5 cm between the center of the magnet and the sample position. (**c**) Scanning electron microscopy images of the beam structures after critical point drying. (**d**) The corresponding light microscopic images of the written beam structures in the undeflected (**top**) and maximally deflected states (**bottom**). In the field shown, 49 structures (one printing field) were written in 6 min.

2PC allows for a rather simple variation of the actuator dimensions or aspect ratios. We have investigated the latter and compared our results to simple theoretical predictions using the Euler–Bernoulli beam theory [45]. The written beams have one end fixed to the surface and one free end. By neglecting the torsional motions, a simple cantilever model can be used. Since the nanoparticles are homogeneously distributed in the beam, a uniformly distributed volume load can be assumed. For simplification, this volume load is projected onto a line load q, which is shown schematically in Figure 3a. Thus, the model used now corresponds to a cantilever with a uniformly distributed load. The aim is to determine the maximum deflection at the free end of the beam as a function of the beam structure, i.e., the beam height. An expression for the maximum deflection of the beam can be obtained by integrating twice the ordinary differential equation of the deflection curve. Here, it is assumed that the system

is in the linear elastic range (Hooke's law) and the equation is therefore only valid for small deflections. For the maximum deflection δ of the beam the following formula is obtained:

$$\delta = \frac{q \cdot h^4}{8} \cdot E \cdot I$$

Thus, the maximum deflection of a beam depends on the fourth power of the height of the beam. The dependence of the deflection on the Young's modulus E reflects the material properties. The area moment of inertia I involves the structural properties of the beams and can be described according to:

$$I = \frac{b \cdot a^3}{12}$$

In this expression, the moment of inertia of the area is linearly related to the width b and depends on the cube of the thickness a of the beam. However, changing the width or thickness would also increase the load because the nanoparticles are homogeneously distributed throughout the volume. Since the equation uses the uniformly distributed line load, increasing the thickness or width will not increase the load in the equation. Therefore, in order to obtain the proper dependency of these parameters on deflection, the increase in load due to a change in width or thickness must be projected onto the linear load, as shown in Figure 3b,c. As a result, the deflection δ is independent of the width and inversely proportional to the square of the thickness.

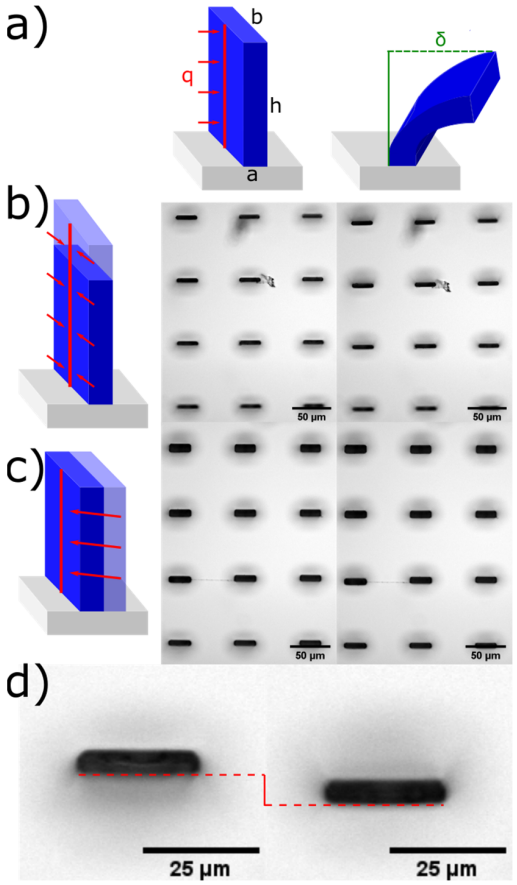

Figure 3. (**a**) Schematic representation of a cantilever beam with a uniformly distributed load and the resulting deflection. The position of the maximum deflection is shown by the green line. Schematic representation and light microscope images of beams which were (**b**) varied in height, increasing the height from 60 to 75 µm in 5 µm steps, and (**c**) varied in thickness, increasing the thickness from 5 to 8 µm in 1 µm steps. The not-deflected structures are shown on the left and the deflected structures on the right. (**d**) Zoomed-in image showing the deflection of a beam with a height of 65 µm.

To verify the results obtained from beam theory, the deflections were determined using light microscopy images (Figure 3b,c). For better visualisation of the actuation, Figure 3c shows a zoomed-in image of the deflection of a beam with a height of 65 µm; in the supporting information videos of the actuation process are shown in Figure 3b,c. (Movies S1 and S2). The obtained deflections were plotted against the respective height h or thickness a. These were then fitted as functions of h and a. Figure 4 shows the fit curves obtained. A good agreement between the measured deflections and the calculated dependencies (solid lines) can be seen. Even for larger deflections in the range of 10 µm (>10% of the height of the structure), the measured deflection agreed well with theory, demonstrating that the simple beam theory is suitable to describe the deflection behavior.

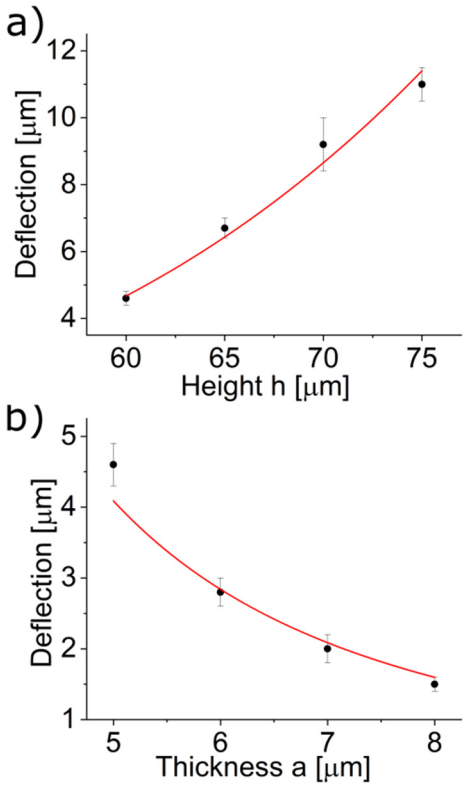

Figure 4. Plot of the deflection against (**a**) the height and (**b**) the width of the beam. The height was fitted proportional to h^4 and the thickness anti-proportional to a^2 according to beam theory.

4. Conclusions

Two-photon crosslinking of a composite consisting of a precursor of an elastic polymer and superparamagnetic particles allows direct writing of flexible 3D micro-magnets of almost any three-dimensional shape with high resolution. A unique feature of this method is that the magnetic micro-actuators are not printed from a liquid monomer containing solution, but from a polymer in the glassy state. This allows the writing of complex systems and large arrays of micro magnets in a very simple way in one step with high yield. Additionally, simple beam theory can be used to predict the deflection behavior of such architectures as a function of actuator dimensions and mechanical properties.

We believe that these findings pave the way for writing of cooperative actuator fields, which allow, among other things, controlled pushing of particles by combinations of movable and non-movable actuators, as well as the generation of metachronal waves and multicomponent micro-actuators.

Supplementary Materials: The following supporting information can be downloaded at: https://www.mdpi.com/article/10.3390/act12030124/s1, Movie S1: Support_Figure3_1.gif, Movie S2: Support_Figure3_2.gif.

Author Contributions: Conceptualization, J.R. and O.P.; methodology, N.G. and J.U.L.; investigation, N.G. and J.U.L.; resources, J.R.; writing—original draft preparation, N.G.; writing—review and editing, N.G., O.P. and J.R.; visualization, N.G. and J.U.L.; supervision, J.R.; funding acquisition, J.R. All authors have read and agreed to the published version of the manuscript.

Funding: This research was funded by Deutsche Forschungsgemeinschaft (DFG, German Research Foundation) under Priority Programme SPP 2206–KOMMMA and partially by the Deutsche Forschungsgemeinschaft (DFG, German Research Foundation) under Germany's Excellence Strategy–EXC-2193/1–390951807.

Data Availability Statement: The data presented in this study are available upon request from the corresponding author. The data are not publicly available because they are part of ongoing research.

Acknowledgments: Natalia Schatz and Martin Schönstein are thanked for valuable technical assistance.

Conflicts of Interest: The authors declare no conflict of interest. The funders had no role in the design of the study; in the collection, analyses, or interpretation of data; in the writing of the manuscript; or in the decision to publish the results.

References

1. den Toonder, J.M.J.; Onck, P.R. Microfluidic manipulation with artificial/bioinspired cilia. *Trends Biotechnol.* **2013**, *31*, 85–91. [CrossRef]
2. Zhang, S.; Wang, Y.; Onck, P.; den Toonder, J.M.J. A concise review of microfluidic particle manipulation methods. *Microfluid. Nanofluidics* **2020**, *24*, 24. [CrossRef]
3. Zhou, H.; Mayorga-Martinez, C.C.; Pané, S.; Zhang, L.; Pumera, M. Magnetically Driven Micro and Nanorobots. *Chem. Rev.* **2021**, *121*, 4999–5041. [CrossRef] [PubMed]
4. Jager, E.W.; Smela, E.; Inganäs, O. Microfabricating Conjugated Polymer Actuators. *Science* **2000**, *290*, 1540–1545. [CrossRef] [PubMed]
5. Sahadevan, V.; Panigrahi, B.; Chen, C.-Y. Microfluidic Applications of Artificial Cilia: Recent Progress, Demonstration, and Future Perspectives. *Micromachines* **2022**, *13*, 735. [CrossRef]
6. Piraux, L. Magnetic Nanowires. *Appl. Sci.* **2020**, *10*, 1832. [CrossRef]
7. Venkata Kamalakar, M.; Raychaudhuri, A.K. Resistance anomaly near phase transition in confined ferromagnetic nanowires. *Phys. Rev. B* **2010**, *82*, 195425. [CrossRef]
8. Toonder, J.M.J.; Bos, F.; Broer, D.; Filippini, L.; Gillies, M.; de Goede, J.; Mol, T.; Reijme, M.; Talen, W.; Wilderbeek, H.; et al. Artificial cilia for active micro-fluidic mixing. *Lab Chip* **2008**, *8*, 533–541. [CrossRef]
9. van Oosten, C.L.; Bastiaansen, C.W.M.; Broer, D.J. Printed artificial cilia from liquid-crystal network actuators modularly driven by light. *Nat. Mater.* **2009**, *8*, 677. [CrossRef]
10. Li, M.; Kim, T.; Guidetti, G.; Wang, Y.; Omenetto, F.G. Optomechanically Actuated Microcilia for Locally Reconfigurable Surfaces. *Adv. Mater.* **2020**, *32*, 2004147. [CrossRef]
11. Oh, K.; Chung, J.-H.; Devasia, S.; Riley, J.J. Bio-mimetic silicone cilia for microfluidic manipulation. *Lab Chip* **2009**, *9*, 1561. [CrossRef]
12. Timonen, J.V.I.; Johans, C.; Kontturi, K.; Walther, A.; Ikkala, O.; Ras, R.H.A. A Facile Template-Free Approach to Magnetodriven, Multifunctional Artificial Cilia. *ACS Appl. Mater. Interfaces* **2010**, *2*, 2226–2230. [CrossRef] [PubMed]
13. Islam, T.U.; Bellouard, Y.; den Toonder, J.M.J. Highly motile nanoscale magnetic artificial cilia. *Proc. Natl. Acad. Sci. USA* **2021**, *118*, e2104930118. [CrossRef] [PubMed]
14. Belardi, J.; Schorr, N.; Prucker, O.; Rühe, J. Artificial Cilia: Generation of Magnetic Actuators in Microfluidic Systems. *Adv. Funct. Mater.* **2011**, *21*, 3314–3320. [CrossRef]
15. Hanasoge, S.; Ballard, M.; Hesketh, P.J.; Alexeev, A. Asymmetric motion of magnetically actuated artificial cilia. *Lab Chip* **2017**, *17*, 3138–3145. [CrossRef] [PubMed]
16. Zhang, S.; Zhang, R.; Wang, Y.; Onck, P.R.; den Toonder, J.M.J. Controlled Multidirectional Particle Transportation by Magnetic Artificial Cilia. *ACS Nano* **2020**, *14*, 10313. [CrossRef] [PubMed]
17. Judith, R.M.; Fisher, J.K.; Spero, R.C.; Fiser, B.L.; Turner, A.; Oberhardt, B.; Taylor, R.M.; Falvo, R.; Superfine, R. Micro-elastometry on whole blood clots using actuated surface-attached posts (ASAPs). *Lab Chip* **2015**, *15*, 1385. [CrossRef] [PubMed]
18. Fahrni, F.; Prins, M.W.J.; van Ijzendoorn, L.J. Micro-fluidic actuation using magnetic artificial cilia. *Lab Chip* **2009**, *9*, 3413–3421. [CrossRef]
19. Evans, B.A.; Shields, A.R.; Carroll, R.L.; Washburn, S.; Falvo, M.R.; Superfine, R. Magnetically actuated nanorod arrays as biomimetic cilia. *Nano Lett.* **2007**, *7*, 1428–1434. [CrossRef]
20. Khaderi, S.N.; den Toonder, J.M.J.; Onck, P.R. Magnetically Actuated Artificial Cilia: The Effect of Fluid Inertia. *Langmuir* **2012**, *28*, 7921–7937. [CrossRef]
21. Zhou, Z.-g.; Liu, Z.-w. Biomimetic Cilia Based on MEMS Technology. *J. Bionic. Eng.* **2008**, *5*, 358. [CrossRef]

22. Hussong, J.; Schorr, N.; Belardi, J.; Prucker, O.; Rühe, J.; Westerweel, J. Experimental investigation of the flow induced by artificial cilia. *Lab Chip* **2011**, *11*, 2017–2022. [CrossRef] [PubMed]
23. Khaderi, S.N.; Craus, C.B.; Hussong, J.; Schorr, N.; Belardi, J.; Westerweel, J.; Prucker, O.; Rühe, J.; den Toonder, J.M.J.; Onck, P.R. Magnetically-actuated artificial cilia for microfluidic propulsion. *Lab Chip* **2011**, *11*, 2002–2010. [CrossRef] [PubMed]
24. Heckele, M.; Schomburg, W.K. Review on micro molding of thermoplastic polymers. *J. Micromech. Microeng.* **2004**, *14*, R1–R14. [CrossRef]
25. Pawlicki, M.; Collins, H.A.; Denning, R.G.; Anderson, H.L. Two-Photon Absorption and the Design of Two-Photon Dyes. *Angew. Chem.* **2009**, *121*, 3292. [CrossRef]
26. LaFratta, C.N.; Fourkas, J.T.; Baldacchini, T.; Farrer, R.A. Multiphoton fabrication. *Angew. Chem. Int. Ed.* **2007**, *46*, 6238. [CrossRef]
27. Park, S.-H.; Yang, D.-Y.; Lee, K.-S. Two-photon stereolithography for realizing ultraprecise three-dimensional nano/microdevices. *Laser Photon- Rev.* **2009**, *3*, 1–11. [CrossRef]
28. Coenjarts, C.A.; Ober, C.K. Two-Photon Three-Dimensional Microfabrication of Poly(Dimethylsiloxane) Elastomers. *Chem. Mater.* **2004**, *16*, 5556–5558. [CrossRef]
29. Montemayor, L.C.; Meza, L.R.; Greer, J.R. Design and Fabrication of Hollow Rigid Nanolattices via Two-Photon Lithography. *Adv. Eng. Mater.* **2014**, *16*, 184–189. [CrossRef]
30. Dayan, C.B.; Chun, S.; Krishna-Subbaiah, N.; Drotlef, D.-M.; Akolpoglu, M.B.; Sitti, M. 3D Printing of Elastomeric Bioinspired Complex Adhesive Microstructures. *Adv. Mater.* **2021**, *33*, e2103826. [CrossRef]
31. Wu, S.; Serbin, J.; Gu, M. Two-photon polymerisation for three-dimensional micro-fabrication. *J. Photochem. Photobiol. A* **2006**, *181*, 1–11. [CrossRef]
32. Faraji Rad, Z.; Prewett, P.D.; Davies, G.J. High-resolution two-photon polymerization: The most versatile technique for the fabrication of microneedle arrays. *Microsyst. Nanoeng.* **2021**, *7*, 71. [CrossRef] [PubMed]
33. Lee, K.-S.; Kim, R.H.; Yang, D.-Y.; Park, S.H. Advances in 3D nano/microfabrication using two-photon initiated polymerization. *Prog. Polym. Sci.* **2008**, *33*, 631. [CrossRef]
34. Wang, X.; Qin, X.-H.; Hu, C.; Terzopoulou, A.; Chen, X.-Z.; Huang, T.-Y.; Maniura-Weber, K.; Pané, S.; Nelson, B.J. 3D Printed Enzymatically Biodegradable Soft Helical Microswimmers. *Adv. Funct. Mater.* **2018**, *28*, 1804107. [CrossRef]
35. Giltinan, J.; Sridhar, V.; Bozuyuk, U.; Sheehan, D.; Sitti, M. 3D Microprinting of Iron Platinum Nanoparticle-Based Magnetic Mobile Microrobots. *Adv. Intell. Syst.* **2021**, *3*, 2000204. [CrossRef]
36. Peters, C.; Ergeneman, O.; García, P.D.W.; Müller, M.; Pané, S.; Nelson, B.J.; Hierold, C. Superparamagnetic Twist-Type Actuators with Shape-Independent Magnetic Properties and Surface Functionalization for Advanced Biomedical Applications. *Adv. Funct. Mater.* **2014**, *24*, 5269. [CrossRef]
37. Xia, H.; Wang, J.; Tian, Y.; Chen, Q.-D.; Du, X.-B.; Zhang, Y.-L.; He, Y.; Sun, H.-B. Ferrofluids for Fabrication of Remotely Controllable Micro-Nanomachines by Two-Photon Polymerization. *Adv. Mater.* **2010**, *22*, 3204. [CrossRef]
38. Wang, J.; Xia, H.; Xu, B.-B.; Niu, L.-G.; Wu, D.; Chen, Q.-D.; Sun, H.-B. Remote manipulation of micronanomachines containing magnetic nanoparticles. *Opt. Lett.* **2009**, *34*, 581–583. [CrossRef]
39. Schwärzle, D.; Hou, X.; Prucker, O.; Rühe, J. Polymer Microstructures through Two-Photon Crosslinking. *Adv. Mater.* **2017**, *29*, 1703469. [CrossRef]
40. Schuh, K.; Prucker, O.; Rühe, J. Tailor-Made Polymer Multilayers. *Adv. Funct. Mater.* **2013**, *23*, 6019–6023. [CrossRef]
41. Prucker, O.; Brandstetter, T.; Rühe, J. Surface-attached hydrogel coatings via C,H insertion crosslinking for biomedical and bioanalytical applications (Review). *Biointerphases* **2017**, *13*, 10801. [CrossRef] [PubMed]
42. Kanokwijitsilp, T.; Körner, M.; Prucker, O.; Anton, A.; Lübke, J.; Rühe, J. Kinetics of Photocrosslinking and Surface Attachment of Thick Polymer Films. *Macromolecules* **2021**, *54*, 6238. [CrossRef]
43. Kotrade, P.F.; Rühe, J. Malonic Acid Diazoesters for C−H Insertion Crosslinking (CHic) Reactions: A Versatile Method for the Generation of Tailor-Made Surfaces. *Angew. Chem. Int. Ed.* **2017**, *56*, 14405–14410. [CrossRef]
44. Li, X.-F. A unified approach for analyzing static and dynamic behaviors of functionally graded Timoshenko and Euler–Bernoulli beams. *J. Sound Vib.* **2008**, *318*, 1210–1229. [CrossRef]
45. Gere, J.M.; Goddno, B.J. *Mechanics of Materials, Brief Edition*; Cengage Learning: Stamford, CT, USA, 2012; pp. 480–492.
46. Grespan, E.; Martewicz, S.; Serena, E.; Le Houerou, V.; Rühe, J.; Elvassore, N. Analysis of calcium transients and uniaxial contraction force in single human embryonic stem cell-derived cardiomyocytes on microstructured elastic substrate with spatially controlled surface chemistries. *Langmuir* **2016**, *32*, 12190–12201. [CrossRef] [PubMed]